

## Large Eddy Simulations for Floating Wind Turbine Under Complex Atmospheric Inflow

Shun Xu<sup>1</sup>, Nina Wang<sup>2</sup>, Decheng Wan<sup>1\*</sup>, Sergei Strijhak<sup>3</sup>

<sup>1</sup> Computational Marine Hydrodynamics Lab (CMHL), School of Naval Architecture, Ocean and Civil Engineering, Shanghai Jiao Tong University, Shanghai, China

<sup>2</sup> Key Laboratory of Far-shore Wind Power Technology of Zhejiang Province, Huadong Engineering Corporation Limited, Hangzhou, China

<sup>3</sup> Ivannikov Institute for System Programming of the Russian Academy of Sciences, Moscow, Russia

\*Corresponding author

### ABSTRACT

The development of wind turbine towards to larger-scale and floating type, leading to the significant impact on the aerodynamic performance and fatigue load of the wind turbine induced by the complex atmospheric inflow. In this study, the numerical investigation of floating wind turbine (FOWT) under complex atmospheric boundary layer (ABL) inflow is performed. The NREL 5MW reference turbine mounted on the OC4 floating platform is adopted as the research object. Large eddy simulations (LES) combined with the actuator line model is used for the wind turbine blades numerical simulation, and the platform motions are solved by the potential theory. The complex ABL inflow is generated using a precursor LES method with long-enough time to obtain the quasi-equilibrium state turbulence. And the calculation results are compared with the uniform wind inflow. The oscillation amplitude of the rotor power for FOWT under uniform inflow does not exceed 40% with the excitation of regular incident wave, while the amplitude for ABL inflow reaches up to 100%. Long-term significant response of rotor power is observed because of the large-scale high-velocity airflow upstream the turbine rotor plane. The later asymmetric distribution of ABL inflow velocity is responsible for evidently response of aerodynamic yaw moment amplitude. For the floating platform motions, the oscillating amplitude of yaw motion for ABL inflow is over 2°, while the output value for uniform inflow is steady and does not exceed 0.2°. The differences of the other five platform motions are not significantly observed.

**KEY WORDS:** floating wind turbine; atmospheric boundary layer; larger eddy simulations; actuator line model; precursor simulation.

### INTRODUCTION

In recent years, the traditional fossil resources are gradually difficult to meet the significant demand of energy with the greatly development of society. However, wind energy has received increasing attention due to the properties of non-polluting, renewable and large reserves<sup>[1]</sup>, which is responsible for the prosper growth of the wind turbine technology. According to the 2021 Global Wind Energy Report<sup>[2]</sup>, the installed

capacity of wind turbine in 2020 reached up to 93GW, resulting 53% growing compared with the last year. The development trend of wind turbine is gradually towards to large-scale and floating type, leading to the significant impact on the aerodynamic performance and fatigue load of the wind turbine induced by the complex atmospheric boundary layer (ABL) inflow. Therefore, the numerical simulation for studying the operation performance of FOWT under the complex ABL inflow is very necessary.

The complex ABL inflow on the onshore wind turbine has been widely researched. Churchfield et al.<sup>[3]</sup> incorporate the large eddy simulations (LES) and actuator line model (ALM) to present a numerical study of atmospheric and turbine wakes on wind turbine dynamics with two different atmospheric stability and surface roughness, they point out that the turbulence structures generated in the ABL can cause the isolated loading events as significant as when wind turbine waked by a upstream turbine. Lee et al.<sup>[4]</sup> study the effects of atmospheric stability and surface roughness on wind turbine fatigue load, the results show that the two parameters have evidently impacts on turbine fatigue load. Lu et al.<sup>[5]</sup> investigate the characteristics of wind turbine wakes under a stable boundary layer inflow, they argue that a skewed spatial structure is caused by the Coriolis force and a part of turbulence energy is driven away from the center of turbine wakes. Ning and Wan<sup>[6]</sup> investigate the wake meandering and its effects to wind turbulence aerodynamics.

Compared with the onshore wind turbine, the inflow wind conditions are more simplified on the FOWT. Cheng et al.<sup>[7]</sup> perform the fully coupled aero-hydrodynamic responses of a FOWT with the combined uniform wind inflow and regular incident wave. In order to consider the properties of ABL inflow, the shear wind inflow is adopted for the FOWT, and the wind turbine blades are modeled by the ALM method<sup>[8]</sup>. However, the wind turbine aerodynamic performance is significantly affected by the complex ABL inflow due to the large-scale development of wind turbine blades. Li et al.<sup>[9]</sup> study the effects of wind fields to FOWT aerodynamic performance, and the thrust force and power generation become very unstable because of the presence of turbulence wind fields. Johlas et al.<sup>[10,11]</sup> examine the turbine wake characteristics of FOWT in complex ABL inflow and the effects of different platforms to wake characteristics and platform motions.

In the present study, the numerical simulation of FOWT under complex ABL inflow is investigated. The LES method incorporated with the ALM is adopted to investigate the aerodynamic performance of FOWT,

and the complex ABL inflow generated by the long-term LES simulation is used for the inflow wind condition. The platform responses are solved using the potential theory, and the actuator point positions and relative inflow velocities are delivered in the coupling processes between SOWFA and FAST.

## NUMERICAL METHODS

### Actuator Line Model

The wind turbine blades are modeled based on the actuator line model (ALM), which the blade surface boundary layer is not resolved. The ALM do not need expensive computational cost and the satisfied numerical results are also obtained, compared with the blade boundary layer mesh resolved method. This ALM was first proposed by the Sørensen and Shen <sup>[12]</sup>, the basic idea is to employ actuator points representing the radial discretized wind turbine blades. The body force of each actuator point is calculated based on the blade element method, then the body force reacts on flow fields to reflect the influence of wind turbine blades on the flow fields. The body force of actuator point can be expressed by:

$$f = (L, D) = \frac{1}{2} \rho U_{rel}^2 c dr (C_L \bar{e}_L + C_D \bar{e}_D) \quad (1)$$

Where,  $L$  and  $D$  are the lift and drag force of blade element located on the blade radius  $r$ ;  $\rho$  denotes the air density;  $U_{rel}$  represents the relative inflow velocity;  $c$  is the chord length of two-dimensional airfoil;  $dr$  is the width of blade element;  $C_L$  and  $C_D$  denote the lift and drag coefficients, which determined by the local attack angle;  $\bar{e}_L$  and  $\bar{e}_D$  are the unit vectors of lift and drag force directions.

Figure 1 shows the velocity vectors of two-dimensional blade element airfoil, the relative inflow velocity  $U_{rel}$  can be obtained by the following formulation:

$$U_{rel} = \sqrt{U_z^2 + (\Omega r - U_\theta)^2} \quad (2)$$

Inflow angle  $\phi$  is determined by the inflow conditions, the local attack angle  $\alpha$  equals to the difference of inflow angle  $\phi$  and local pitch angle  $\gamma$ . Besides, the added inflow velocity induced by the platform motions should be considered when modeling the FOWT blades.

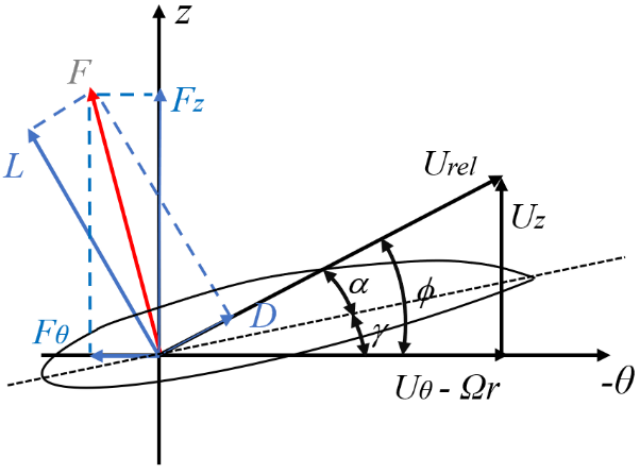


Fig.1 Velocity vectors of two-dimensional airfoil

The body force directly reacting on the flow fields will produce the numerical singularity. Therefore, the Gauss kernel function is adopted on the projection of body force to flow fields. Smooth body force projection can be calculated by:

$$f_\varepsilon = f \otimes \eta_\varepsilon = \sum_{i=1}^N f_i(x_i, y_i, z_i, t) \frac{1}{\varepsilon^3 \pi^2} \exp \left[ -\left( \frac{d_i}{\varepsilon} \right)^2 \right] \quad (3)$$

Where,  $N$  is the number of actuator points;  $(x_i, y_i, z_i)$  denotes the position of  $i$ -th actuator point;  $d_i$  is the distance between the actuator point and projection point;  $\varepsilon$  is the projection width, we in here set  $\varepsilon \approx 2\Delta x$  <sup>[13]</sup> to guarantee the numerical stability;  $\Delta x$  represents the mesh scale around the wind turbine blades.

### Governing Equations

The LES combined with the ALM is performed to study the aerodynamic performance of wind turbine blades. The spatial flited governing equations can be expressed as follows:

$$\begin{aligned} \frac{\partial \bar{u}_i}{\partial x_i} &= 0 \quad (4) \\ \frac{\partial \bar{u}_i}{\partial t} + \frac{\partial}{\partial x_j} (\bar{u}_j \bar{u}_i) &= - \frac{\partial \bar{p}}{\partial x_i} - \frac{1}{\rho_0} \frac{\partial}{\partial x_i} \bar{p}_0(x, y) \\ &\quad - \frac{2\varepsilon_{i3k} \Omega_3 \bar{u}_k}{III} + g \left( \frac{\bar{\theta} - \theta_0}{\theta_0} \right) \delta_{i3} - \frac{\partial}{\partial x_j} (\tau_{ij}^D) + \frac{1}{\rho_0} f_i^T \end{aligned} \quad (5)$$

where, the term I of momentum equation right side is the modified pressure gradient; term II is the background pressure gradient to overcome the bottom surface roughness and drive the generation of ABL inflow; term III is the Corioils force, representing the impact of earth rotation on ABL flow fields; term IV is the buoyancy force driven by the temperature; term V is the tensor of fluid stress, which is calculated by the Smagorinsky sub-scale model; term VI is the body force of wind turbine blades, needed in the successor stage when the wind turbine subjected to the ABL inflow. In addition, the temperature transportation equation should be resolved to obtain the temperature fields:

$$\frac{\partial \bar{\theta}}{\partial t} + \frac{\partial}{\partial x_j} (u_j \bar{\theta}) = - \frac{\partial}{\partial x_j} (q_j) \quad (6)$$

The heat flux  $q_j$  is calculated by:

$$q_j = - \frac{v_{SGS}}{Pr_t} \frac{\partial \bar{\theta}}{\partial x_j} \quad (7)$$

where,  $Pr_t$  is the Prandtl number, taken to be 1/3 in the stability of neutral and convection, more details about the governing equations should refer to literature <sup>[3]</sup>. As for uniform inflow case, the Corioils force and temperature term are not take into consideration, and the background pressure gradient is also not needed.

### Coupling Procedure

As aforementioned, the FOWT aerodynamic performance is simulated based on computational fluid dynamics method, the coupled LES and ALM method is implemented in the OpenFOAM. The potential theory is applied for the hydrodynamic solution, implemented in the FAST HydroDyn and MoorDyn modules. Figure 2 illustrates the coupling procedure between the OpenFOAM and FAST. During the numerical simulation, OpenFOAM solves the aerodynamic flow field and the relative inflow wind velocities at the blade actuator points are delivered to FAST. Then the blade rotation is calculated utilized by the FAST AeroDyn module, and the HydroDyn and MoorDyn modules are used to

solve the FOWT hydrodynamic responses. The blade actuator point positions considering the floating platform motions are feedback to the OpenFOAM. The whole coupling procedure is implemented in the opensource software SOWFA.

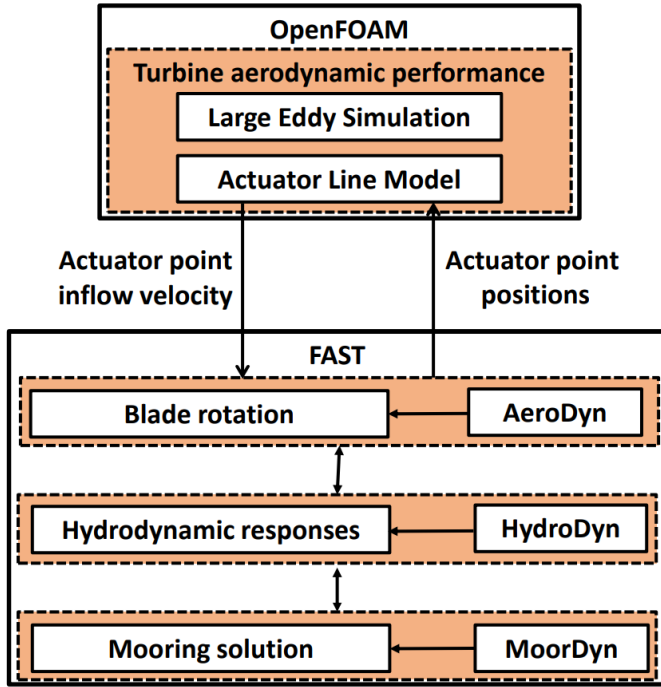


Fig.2 Coupling procedure of FOWT

## COMPUTATION SET UP

### Model Description

The OC4 DeepCwind semisubmersible concept<sup>[14]</sup> is adopted in this work. The wind turbine is the NREL 5MW baseline wind turbine<sup>[15]</sup>, which is a traditional three blades wind turbine incorporates a variable-speed torque controller and a blade pitch controller to regulate the power generation based on the operational state. Table 1 shows the main parameters of the wind turbine.

Table 1. Main parameters of NREL 5MW wind turbine

Term	Value
Rated power	5 MW
Rated wind velocity	11.4 m/s
Rated rotor velocity	12.1 rpm
Hub height	90 m
Blade number	3

A three-column submersible platform is used to carry the wind turbine. The platform is made up of three main offset columns inducing buoyance and restoring force, one central column supporting the wind turbine, as well as a series of diagonal cross and horizontal bracing components. Three mooring lines oriented symmetrically at 60°, 180°, 300° are applied to limit platform displacement. The relevant properties of floating platform and mooring system are outlined in Table 2.

### ABL inflow

The precursor-successor strategy is performed for the numerical

simulation of FOWT aerodynamic performance with the condition of ABL inflow. In the precursor stage, the complex ABL inflow is induced by the bottom surface roughness in the long-term simulation process. As illustrated in Figure 3, the periodic boundary conditions are used on the four side walls of the computational region to save the computational costs by inducing the size of calculation domain. The top of the computational domain is set as the slip boundary condition, and the bottom boundary adopts the Moeng wall function model<sup>[16]</sup>, which the surface roughness is set to 0.001 representing the typical offshore condition. The length, width and height of the calculation region are 5000m, 1000m and 1000m, respectively. And the grid resolution in three directions is 10m×10m×10m, corresponding to 5 million grids. The wind velocity and wind direction at the hub height are set to 11.4 m/s rated inflow velocity and 270° (along with the x axis).

Table 2. Properties of floating platform and mooring system

Term	Value
Draft	20 m
Platform mass	13,473,000 kg
Displacement	13,986.8 m <sup>3</sup>
Centre of mass	(0 m, 0 m, -13.5 m)
Platform roll inertia	6.827×10 <sup>9</sup> kg·m <sup>2</sup>
Platform pitch inertia	6.827×10 <sup>9</sup> kg·m <sup>2</sup>
Platform yaw inertia	1.226×10 <sup>10</sup> kg·m <sup>2</sup>
Depth to anchor	200 m
Depth to fairlead	14 m
Mooring line diameter	0.0766 m
Equivalent line mass density	113.35 kg/m
Equivalent mooring line extensional stiffness	753.6 MN

For the configuration of initial potential temperature fields, setting 300K uniform distribution from the bottom to 700m height. The temperature inversion layer from 700m to 800m height is used to limit the generation of atmospheric boundary layer height, which the temperature linearly increases to 308K. As for the 800m to 1000m height, the temperature linearly increases at a rate of 0.003K/m. And the neutral atmospheric heat stability is performed for the precursor stage. The numerical simulation time is 18800s for the precursor stage to generate the quasi-equilibrium state atmospheric turbulence, and the calculation step is 0.4s. The inflow data in the last 800s are reserved as the input of the successor stage.

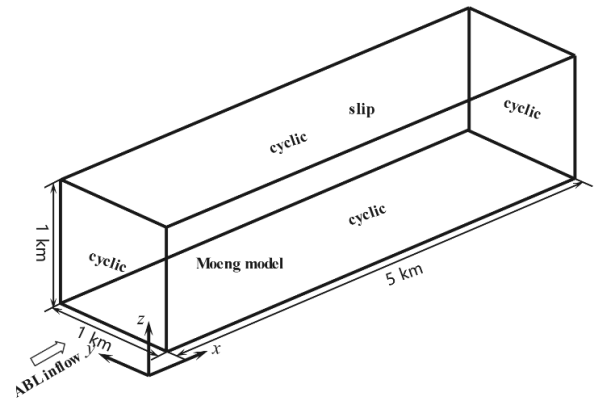


Fig.3 Calculation region of precursor stage

In the successor stage, the FOWT is subjected to the complex ABL inflow. The north and east sidewall boundaries are modified to zero gradient boundary conditions to prevent downstream wind turbine wake cyclically entering to the upstream boundary. Figure 4 illustrates the

meshing strategy of the successor stage. The wind turbine is located downstream 500m of the upper inflow boundary. The properties of background mesh are the same as the precursor stage, corresponding to the 10m×10m×10m mesh resolution. Two-level mesh refinement strategy is used around the wind turbine domain to accurately capture the details of the flow fields. The properties of the two mesh refinement areas

are 1400m×500m×270m and 1200m×300m×220m, and the distance between the wind turbine and the two mesh refinement areas upstream boundaries are 200m and 100m, respectively. The mesh number after refinement is 10.8 million. Simulation time and time step are 800s and 0.02s for successor stage, respectively. More details about the mesh refinement strategy can be found in references [6, 7, 17].

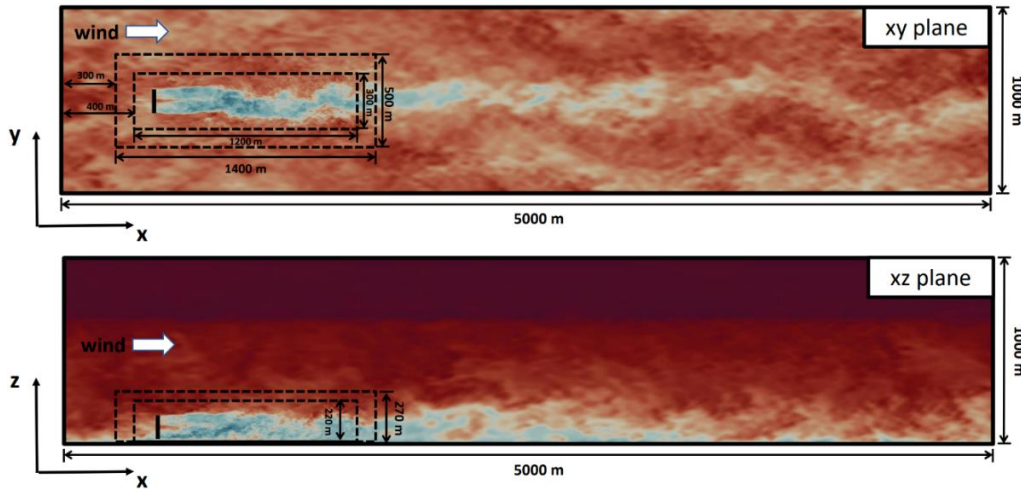


Fig.4 Mesh refinement configuration of successor stage

### Uniform inflow

Figure 5 shows the mesh refinement strategy of the uniform inflow case for FOWT. The scale of calculation domain is 1260m×378m×378m, and the turbine is located downstream 378m of the upper inflow boundary. The same configuration of background mesh resolution and two-level mesh refinement method are also used for the uniform inflow case, which the refined mesh number is about 3 million. For the boundary conditions, the upstream boundary is the wind velocity inlet boundary condition, corresponding to a uniform inflow with the 11.4 m/s wind velocity and 270° inflow wind direction. The downstream boundary is the free outflow boundary condition, and the four side walls are periodic boundary conditions. Simulation time and time step are 400 s and 0.02 s, respectively.

### Inflow conditions for floating wind turbine

Two different inflow wind conditions are used for the FOWT, corresponding to the neutral boundary layer (NBL) complex inflow with the 11.4m/s wind velocity at hub height and 11.4m/s uniform wind inflow, respectively. For incident wave, the Stokes first order deep water wave is applied for the both numerical cases, which the wave height and

period are 7.58 m and 12.1 s. Table 3 shows the inflow conditions of FOWT, note that the heading angles of wind and wave are both along with x axis.

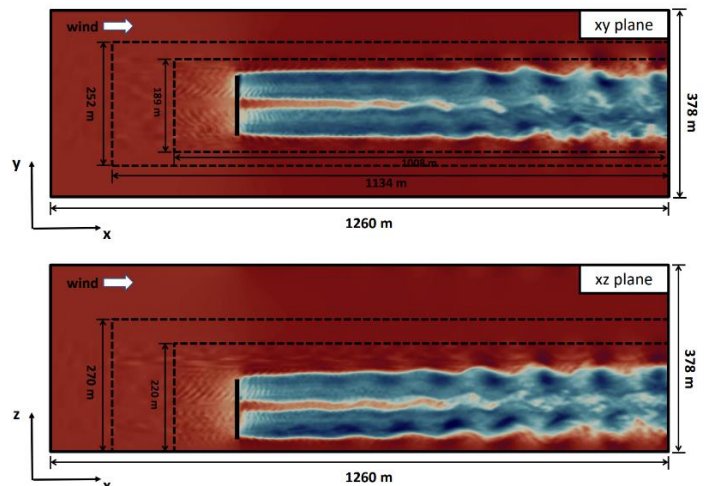


Fig.5 Mesh refinement configuration of uniform inflow case

Table 3. Inflow conditions for FOWT

Case number	Inflow wind		Incident wave		
	Type	Wind velocity	Type	Wave height	Wave period
ABL	NBL complex inflow	11.4 m/s at hub height	Stokes first order deep water wave	7.58 m	12.1 s
Uniform	Uniform inflow	11.4 m/s	Stokes first order deep water wave	7.58 m	12.1 s

## RESULTS AND DISCUSSIONS

### Rotor power

Figure 6 illustrates the aerodynamic power of FOWT for two different inflow wind conditions. The rotor power is normalized using the mean value of rotor power under uniform inflow wind condition with the

calculation time range from 200s to 400s. The oscillation phenomenon of rotor power output values is observed, due to the turbine blade rotation and platform motions induced by the incident wave. Because of the steady property for uniform inflow wind, the oscillation amplitude of the rotor power does not exceed 40%. However, the rotor power time-varying values of ABL inflow condition oscillating significantly, and the oscillation amplitude is reach up to 100%. The high turbulence intensity ABL complex inflow is responsible for the strongly oscillating of the

rotor power. Besides, the normalized rotor power is up to 1.5 near the calculation time 450s and the duration of significant rotor power responses is over 100s, which may be caused by the large-scale turbulent structures the in ABL inflow.

The subplot at bottom right shows the rotor power of 50s time range period. For the uniform inflow wind condition, the rotor power presents periodic variation. The bigger and smaller periods are corresponding to the incident wave period and blade rotation period, respectively. And the max and min values of normalized rotor power are slightly lower than 1.2 and higher than 0.8. Compared with the uniform wind condition, the periodic variation in ABL inflow is also evident. However, the varying amplitude is stronger due to the wind shear effects induced by the sea surface roughness. The smaller rotor power is occurred when two blades locate lower the hub height. Correspondingly, two blades locate higher the hub height is responsible for the higher rotor power. The max and min values of normalized rotor power are slightly higher 1.2 and lower 0.8. In addition, some small bumps caused by the small-scale high intensity turbulence structures are also observed on the power time-varying curve.

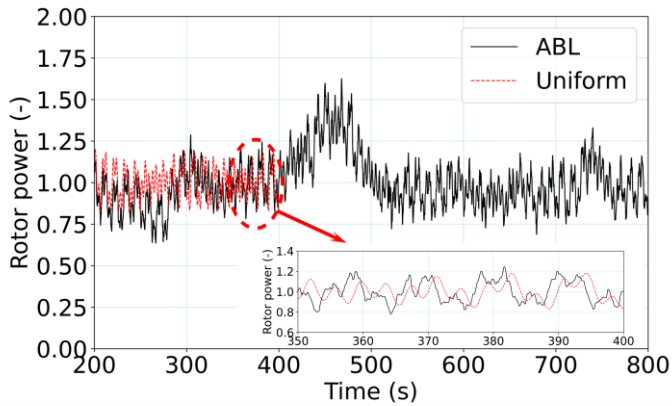


Fig.6 Time-varying curves of rotor power

### Yaw moment

The significant yaw moment will occur with two wind turbine blades on the same side when wind turbine rotating. Figure 7 presents the yaw moment responses of FOWT with two different inflow wind conditions. Similar to the rotor power, the periodic variation of yaw moment corresponding to the incident wave and blade rotation periods is also evident. The amplitude for uniform condition is slighter than the ABL

inflow, and some small bumps are also presented for the ABL inflow. For a large value of yaw moment for ABL inflow, such as at the calculation time 315s, the amplitude tends to decrease with the increasing time. The reason maybe the interaction between floating platform yaw and yaw moment. The platform yaw is induced by the aerodynamic yaw moment, which reducing the yaw moment because the exist of the yaw angle. The decreased yaw moment will induce the decreased platform yaw angle, and the yaw moment tends to increase with the decreased yaw angle.

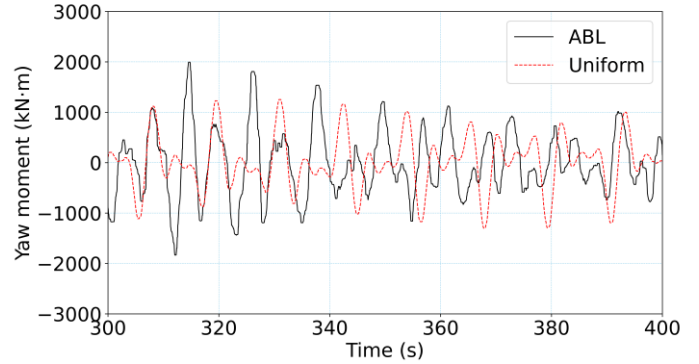
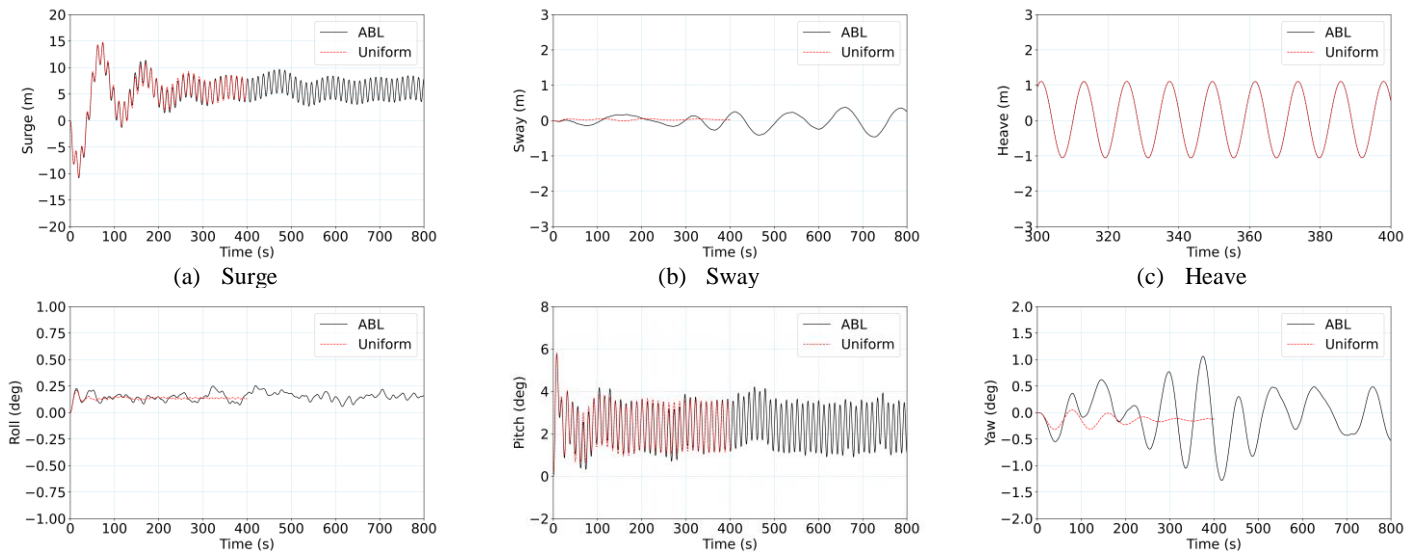


Fig.7 Time-varying curves of yaw moment

### Platform motions

Figure 8 presents the six degrees motions of floating platform with two various inflow wind conditions. There is no difference for the platform heave, because of the small vertical component of the aerodynamic force, compared with the platform wave force. Besides, the platform surge and pitch oscillating at 5m and 2°, respectively. And the minor differences of platform surge and pitch for two inflow wind conditions are observed. For the platform sway and roll, the similar conclusion can also be obtained, while some small oscillations of roll time-varying curve under ABL inflow are presented. Different from the other five platform motions, the platform yaw difference of two various inflow wind conditions is clearly evident. The oscillation amplitude of platform yaw for ABL inflow condition is over 2°, significantly larger than that for uniform inflow. The existing difference of platform yaw maybe induced by the asymmetry of lateral inflow upstream the turbine rotation plane. Overall, the difference of floating platform motions between uniform inflow and ABL inflow is not distinct, due to the large mass and inertia for the OC4 floating platform and stronger mooring tension force [14].



(d) Roll

(e) Pitch

(f) Yaw

Fig.8 Platform motions of FOWT

### Instantaneous flow velocity in ABL inflow

Figure 9 shows the instantaneous flow velocity in wake field of middle vertical plane for ABL case in an incident wave period. Because of the friction effects of the sea surface roughness, the lower velocity of inflow wind near the sea surface is observed. And the large-scale low-velocity airflow is widely distributing from the sea surface to hub height, inducing the significant difference of the aerodynamic pitch moment, compared with the uniform inflow condition. When the airflow passing the wind turbine rotation plane, the lower velocity airflow of turbine wake fields is clearly shown. The wake velocity below the hub height is lower than that above the hub height, due to the large-scale low-velocity wind inflow lower the hub height. With the increased downstream distance,

the lower velocity airflow tends to close the wake center. What's more, the high velocity slender airflow at the rotor center is presented without considering the effects the turbine nacelle. Because of the combined influence of the floating platform pitch motion and the velocity shear between the turbine wake and atmospheric inflow, the wake meandering effects is observed as marked using the red dotted circle in the subfigure (d), which resulting the wake curling phenomenon with the development of turbine wake towards the downstream. And the similar effect is also shown for the high velocity slender airflow at the rotor center. At the far wake region, the turbine wake is fully mixed with the ambient atmospheric inflow. However, the turbine wake recovery rate is slow because of the lower ambient atmospheric turbulence intensity in the neutral stability caused by the low sea surface roughness.

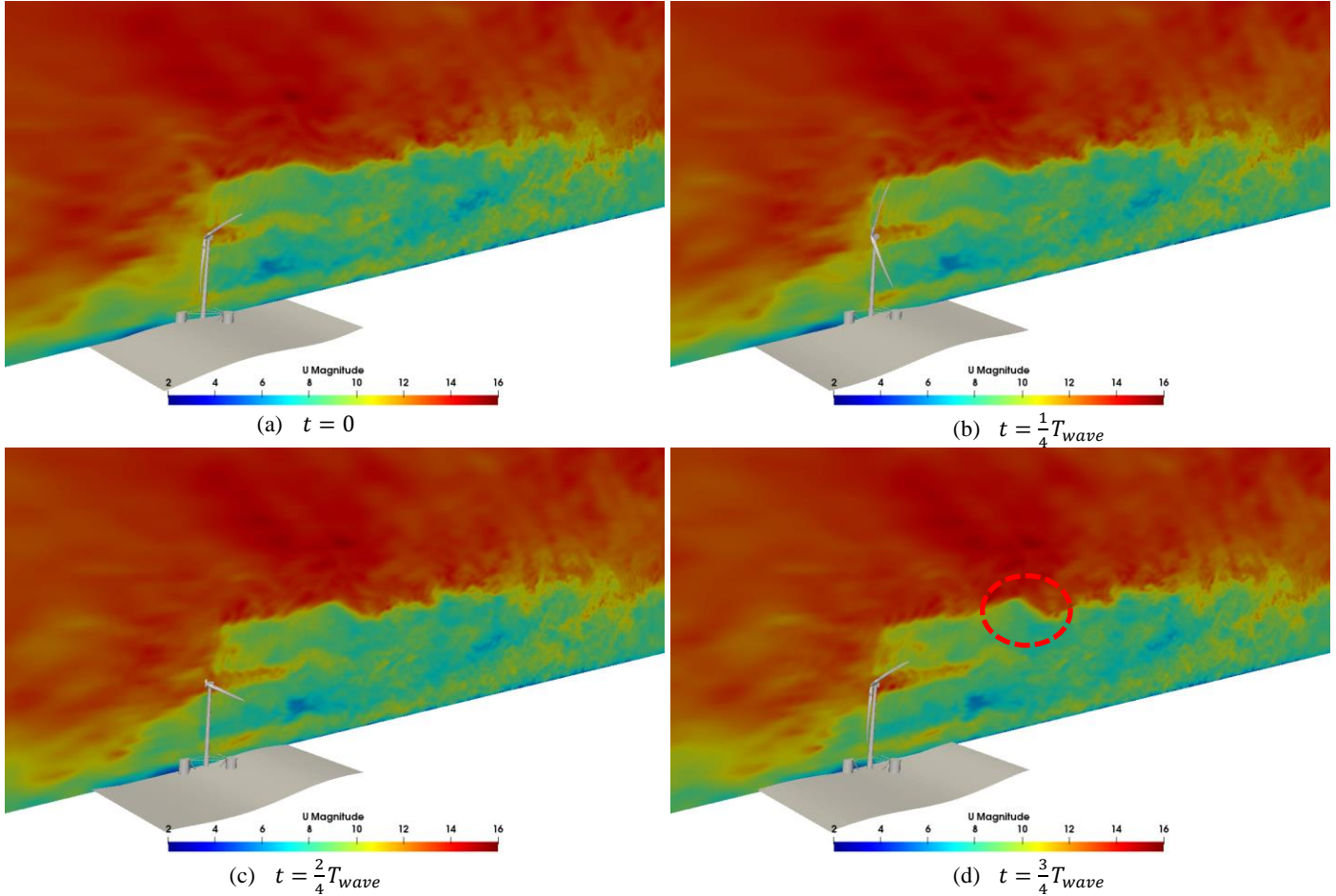


Fig.9 Instantaneous flow velocity in wake field of middle vertical plane for ABL case in an incident wave period

Figure 10 presents the instantaneous velocity contour of hub height plane for ABL case in an incident wave period. As is shown, the lower and higher velocity airflow are both visualized, denoting the complex properties of ABL inflow wind condition. The large-scale high-velocity airflow is visualized upstream the turbine rotor plane, which inducing the long-term significant response of rotor power as mentioned above. And the airflow velocity asymmetric distribution at the turbine rotation plane

is responsible for the evident difference between the ABL and uniform inflows. The turbine wake expansion effect in near wake and meandering effect in far wake are clearly presented, resulting from the interaction between turbine wake and ambient atmospheric inflow. And the wake velocity in far wake region is slow, reflecting the lower wake velocity recovery rate due to the lower sea surface roughness, which consistent with the analysis of Figure 9.

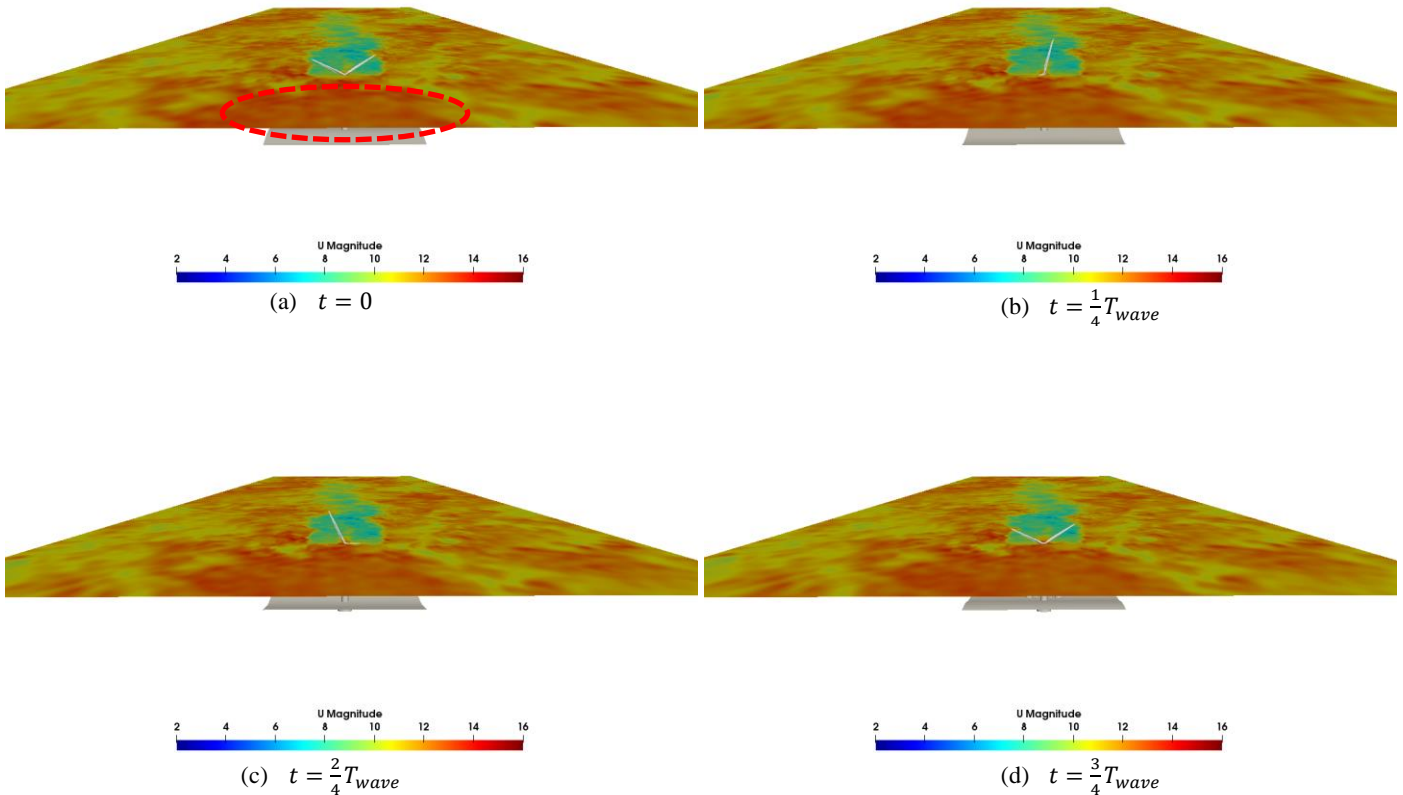


Fig.10 Instantaneous flow velocity in wake field of hub height plane for ABL case in an incident wave period

## CONCLUSIONS

In this research, the NREL 5MW reference wind turbine mounted on the OC4 floating platform is adopted as the research object. The numerical investigation of the FOWT is performed considering two different inflow wind conditions (ABL and uniform inflows). According to the analysis of numerical results for aerodynamic rotor power, yaw moment, floating platform motions and wake velocity fields, some conclusions are obtained as follows.

Because of the steady property for uniform inflow wind, the oscillation amplitude of the rotor power for FOWT does not exceed 40% with the effects of regular incident wave, while the oscillation amplitude for ABL inflow condition reaches up to 100%. Besides, the long-term significant response of rotor power is evident because of the large-scale high-velocity airflow upstream the turbine rotor plane.

The later asymmetric distribution of ABL inflow velocity at rotation plane is responsible for the difference of aerodynamic yaw moment oscillation amplitude with the two various inflow wind conditions. And there are some bumps on the yaw moment time-varying curve for the ABL inflow due to the small-scale turbulence structures.

The difference of floating platform yaw motion with two inflow wind conditions is evident. And the oscillating amplitude for ABL inflow is over  $2^\circ$ , while the output value for uniform inflow is steady and does not exceed  $0.2^\circ$ . The differences of the other five platform motions are not significantly observed, owing to the large mass and inertia for the OC4 floating platform and stronger mooring tension force. As for the instantaneous velocity fields, the wake curling effect is visualized due to the combined interaction of the floating platform pitch motion and the

velocity shear between the turbine wake and atmospheric inflow. Besides, the turbine wake expansion effect in near wake region and meandering effect in far wake are clearly presented.

## ACKNOWLEDGEMENTS

This work was supported by the National Natural Science Foundation of China (51879159, 52131102), and the National Key Research and Development Program of China (2019YFB1704200), to which the authors are most grateful.

## REFERENCES

- Chehouri, A, Younes, R, Ilinca, A, et al (2015). "Review of performance optimization techniques applied to wind turbines," *Applied Energy*, 142: 361-88.
- Cheng, P, Huang, Y, and Wan, D (2019). "A numerical model for fully coupled aero-hydrodynamic analysis of floating offshore wind turbine," *Ocean Engineering*, 173: 183-96.
- Churchfield, M, J, Lee S, Michalakes, J, et al (2012). "A numerical study of the effects of atmospheric and wake turbulence on wind turbine dynamics," *Journal of Turbulence*, (13): N14.
- Council, G, W, E (2021). GWEC| GLOBAL WIND REPORT 2021.
- Huang, Y, Cheng, P, Wan, D (2019). "Numerical analysis of a floating offshore wind turbine by coupled aero-hydrodynamic simulation," *Journal of Marine Science and Application*, 18(1): 82-92.

- Huang, Y, Wan, D (2020). "Investigation of interference effects between wind turbine and spar-type floating platform under combined wind-wave excitation," *Sustainability*, 12(1): 246.
- Johlas, H, Martínez-Tossas, L, Lackner, M, et al (2020). "Large eddy simulations of offshore wind turbine wakes for two floating platform types," *Journal of Physics: Conference Series*. IOP Publishing, 1452(1): 012034.
- Johlas, H, Martinez, L, Schmidt, D, et al (2019). "Large eddy simulations of floating offshore wind turbine wakes with coupled platform motion," National Renewable Energy Lab.(NREL), Golden, CO (United States).
- Jonkman, J, Butterfield, S, Musial, W, et al (2009). "Definition of a 5-MW reference wind turbine for offshore system development," National Renewable Energy Lab.(NREL), Golden, CO (United States).
- Lee, S, Churchfield, M, Moriarty, P, et al (2012). "Atmospheric and wake turbulence impacts on wind turbine fatigue loadings," *proceedings of the 50th AIAA Aerospace Sciences Meeting including the New Horizons Forum and Aerospace Exposition*, F.
- Li, L, Liu, Y, Yuan, Z, et al (2018). "Wind field effect on the power generation and aerodynamic performance of offshore floating wind turbines," *Energy*, 157(AUG.15): 379-90.
- Lu, H and Porté-Agel, F (2011). "Large-eddy simulation of a very large wind farm in a stable atmospheric boundary layer," *Physics of Fluids*, 23(6): 25-2042.
- Moeng, C-H (1984). "A large-eddy-simulation model for the study of planetary boundary-layer turbulence," *Journal of the Atmospheric Sciences*, 41(13): 2052-62.
- Ning, X, Wan, D (2019). "LES Study of wake meandering in different atmospheric stabilities and its effects on wind turbine aerodynamics," *Sustainability*, 11(24): 6939.
- Robertson, A, Jonkman, J, Masciola, M, et al (2014). "Definition of the semisubmersible floating system for phase II of OC4," National Renewable Energy Lab.(NREL), Golden, CO (United States).
- Sorensen, J, N, and Shen, W, Z (2002). "Numerical modeling of wind turbine wakes," *Journal of Fluids Engineering*, 124(2): 393-9.
- Troldborg, N (2009). "Actuator line modeling of wind turbine wakes".